Optimized Hybrid DWT-DCT-SVD Watermarking with Cheetah Optimization Algorithm for Enhanced Imperceptibility and Robustness

Srinivas Pasagadugula * and Venkata Ramanaiah Kota

Department of Electronics and Communication Engineering, Y. S. R. Engineering College (YSREC), Yogi Vemana University, Proddatur, India
Email: srinivasrgv495@gmail.com (S.P.); ramanaiahkota@gmail.com (V.R.K.)
*Corresponding author

***Abstract*—This paper presents a hybrid blind watermarking scheme that integrates 2-level Discrete Wavelet Transform (DWT), Discrete Cosine Transform (DCT), and Singular Value Decomposition (SVD), with embedding strength optimization via the Cheetah Optimization Algorithm (COA). The proposed method achieves exceptional imperceptibility with Peak Signal to Noise Ratio (PSNR) values consistently above 49 dB (reaching up to 57 dB), representing 8–30% improvements over existing methods, while maintaining Structural Similarity Index Measure (SSIM) values above 0.995 and Normalized Cross Correlation (NCC) values near unity (≈1.0000). Comprehensive robustness evaluation demonstrates superior performance against diverse attacks, particularly excelling under geometric distortions and enhancement-based attacks such as histogram equalization (NCC: 0.9902 vs. 0.72 for baseline methods) and sharpening (NCC: 1.0000). The process maintains a moderate watermark capacity of 0.50–1.00 bits per pixel, deliberately optimized for hardware feasibility rather than maximum payload. With reduced computational requirements due to smaller watermark dimensions, the approach achieves embedding and extraction times of 0.2321 s and 0.0227 s, respectively, making it suitable for resource-constrained environments. The COA optimization automatically determines the optimal embedding strength, balancing imperceptibility and robustness. The proposed framework demonstrates consistent superiority across multiple benchmark comparisons, making it highly suitable for real-time applications and future Field Programmable Gate Array (FPGA)/Application Specific Integrated Circuit (ASIC) hardware implementations in secure medical imaging and multimedia protection systems.**

***Keywords*—Discrete Wavelet Transform (DWT), Discrete Cosine Transform (DCT), Singular Value Decomposition (SVD), Cheetah Optimization Algorithm (COA), Peak Signal to Noise Ratio (PSNR), Normalized Cross Correlation (NCC)**

I. Introduction

Digital watermarking has become an essential technique for protecting intellectual property rights, verifying authenticity, and ensuring secure communication within multimedia systems. By subtly embedding identification data into digital content, watermarking offers a balance between invisibility and resilience against common image processing techniques and malicious attacks. A successful watermarking method must demonstrate imperceptibility—ensuring that the watermarked content appears identical to the original—and robustness—maintaining watermark integrity under various deliberate and accidental distortions [1, 2].

Watermarking techniques can generally be divided into spatial-domain and transform-domain methods. While spatial techniques alter pixel intensities directly, they often reduce image quality and are less resistant to compression and filtering. Transform-domain methods, such as the Discrete Cosine Transform (DCT) and Discrete Wavelet Transform (DWT), provide enhanced robustness by embedding data in the frequency coefficients of the host signal [3, 4]. More recent techniques, including the Lifting Wavelet Transform (LWT), Redundant Discrete Wavelet Transform (RDWT), and advanced multi-resolution analysis, further boost stability against noise, compression, and geometric attacks [4, 5]. Notably, RDWT removes the down-sampling step in DWT, ensuring shift invariance and greater robustness to geometric distortions such as rotation, scaling, and translation.

Hybrid watermarking schemes combine the strengths of multiple transforms to utilize complementary properties. For instance, DWT provides spatial-frequency localization, DCT provides high-energy compaction, and Singular Value Decomposition (SVD) ensures the stability of embedded information under various manipulations [4–6]. Numerous studies have shown that

Manuscript received June 11, 2025; revised August 29, 2025; accepted November 20, 2025; published April 16, 2026.

DWT-DCT-SVD and its variants surpass single-transform techniques in terms of the trade-offs between imperceptibility and robustness. Furthermore, emerging frequency–time transforms and multi-stage decomposition strategies, such as double wavelet transforms [3] and RDWT-based hybrids, have demonstrated potential in further improving performance. Recent research also highlights the integration of optimization algorithms to identify optimal embedding parameters, especially the scaling (gain) factor that directly influences visual quality and resilience [4–6]. Approaches using Genetic Algorithms (GA), Particle Swarm Optimization (PSO), Firefly Algorithm, Cuckoo Search, Jaya Optimization, and other evolutionary methods have effectively enhanced robustness against various attacks, including Joint Photographic Experts Group (JPEG) compression, filtering, scaling, rotation, and noise addition. Adaptive embedding guided by perceptual models, such as the Human Visual System (HVS), has also been proposed to minimize perceptual distortion further [6].

For example, a recent RDWT-DCT-SVD watermarking method optimized with the Porcellio Scaber Algorithm (PSA) demonstrated high imperceptibility (PSNR > 50 dB) and robust security (Normalized Cross Correlation (NCC) > 0.98) against standard signal processing and geometric attacks, including Gaussian noise, histogram equalization, median filtering, and scaling [7]. PSA adaptively adjusted the embedding strength factor, surpassing fixed-parameter schemes in both quality and resilience. In PSA-based methods, optimization not only enhances the imperceptibility-robustness balance but also adapts to diverse image contents without manual parameter tuning.

While these approaches demonstrate promise, they reveal a recurring trade-off: methods optimized for imperceptibility often sacrifice robustness, and those designed for robustness exhibit visible distortions. Specifically, RDWT-based schemes achieve very high Peak Signal to Noise Ratio (PSNR) but are unstable to noise and geometric attacks [7]. Conversely, DWT-based methods provide stronger robustness but lower imperceptibility [4]. Optimization techniques such as Jaya, PSO, and distortion correction improve selected metrics, yet their benefits are often attack-specific and computationally intensive [4–6]. Moreover, most prior studies validated their methods on limited datasets, restricting generalizability. This creates a clear gap for a watermarking framework that simultaneously ensures robustness, imperceptibility, and computational efficiency across a wide variety of attacks.

To address these limitations, this study proposes a hybrid DWT-DCT-SVD watermarking method optimized using the Cheetah Optimization Algorithm (COA). The choice of DWT leverages its robustness against signal-processing attacks, while the DCT-SVD combination enhances energy compaction and stability of watermark embedding. COA is employed to adaptively tune the embedding strength adaptively, ensuring an optimal balance between imperceptibility and robustness. Unlike prior works, our approach explicitly emphasizes computational efficiency, making it suitable not only for software simulations but also for future hardware realizations such as Field Programmable Gate Array (FPGA) and Application Specific Integrated Circuit (ASIC) implementations. By combining robustness, imperceptibility, and reduced computational overhead, the proposed scheme provides a practical, hardware-friendly watermarking solution that withstands diverse real-world attack scenarios.

II. Preliminaries

A. Discrete Cosine Transform (DCT)

The Discrete Cosine Transform (DCT) is a fundamental operation that maps an image from the spatial plane to its frequency representation, owing to its strong energy compaction and decorrelation properties [8–10]. It has been extensively applied in image compression and watermarking. The forward and inverse forms of the 2D-DCT can be written as Eqs. (1) and (2).

$$D(p,q) = \frac{2}{\sqrt{AB}}\beta(p)\beta(q) \sum_{i=0}^{A-1}\sum_{j=0}^{B-1} g(i,j)\cos\left(\frac{(2i+1)p\pi}{2A}\right)\cos\left(\frac{(2j+1)q\pi}{2B}\right) \quad (1)$$

$$g(i,j) = \frac{2}{\sqrt{AB}} \sum_{p=0}^{A-1}\sum_{q=0}^{B-1}\beta(p)\beta(q)D(p,q)\cos\left(\frac{(2i+1)p\pi}{2A}\right)\cos\left(\frac{(2j+1)q\pi}{2B}\right) \quad (2)$$

Here, i indicates row index of the image block, j indicates the column index of the image block, $g(i,j)$ denotes the pixel intensities in the spatial image domain. p indicates the vertical frequency index, q indicates the horizontal frequency index, $D(p,q)$ corresponds to the DCT coefficients, $\beta(p)$ normalizes the vertical frequency component, $\beta(q)$ normalizes the horizontal frequency component. The dimensions of each processing block are represented by A and B. The scaling factor is defined as:

$$\beta(r) = \begin{cases} \frac{1}{\sqrt{2}}, & \text{if } r = 0 \\ 1, & \text{otherwise} \end{cases}$$

Here, $\beta(r)$ is the normalization factor used in the DCT to correctly scale the DC coefficient.

B. Discrete Wavelet Transform (DWT)

The Discrete Wavelet Transform (DWT) is a powerful mathematical tool used in image processing for multiresolution analysis, compression, and watermarking [11–13]. Unlike the Fourier transform, which only provides frequency information, the DWT offers both spatial and frequency localization, making it highly suitable for image analysis. In the 2D DWT, the image is decomposed into 4 sub-bands by applying high-pass and low-pass filters, followed by down-sampling.

- Approximation (CA): Low-frequency component containing coarse image details.
- Horizontal detail (CH): High-frequency component capturing horizontal edge information.

- Vertical detail (CV): High-frequency component capturing vertical edges.
- Diagonal detail (CD): High-frequency component capturing diagonal details.

Fig. 1 illustrates the 2-level 2D DWT decomposition process, where the approximation sub band is further decomposed to extract finer details. Fig. 2 illustrates the filtering process, showing how high-pass and low-pass filtering along rows and columns generate the four sub bands.

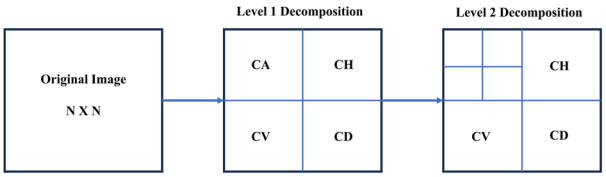

Fig. 1. 2-level 2D DWT decomposition.

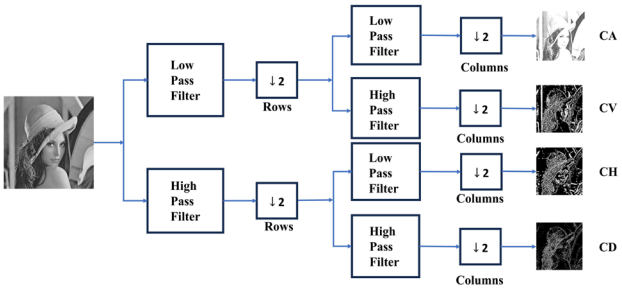

Fig. 2. Filtering-based 2D DWT decomposition process.

C. SVD

If A is a real matrix of size $m \times n$, then it can be factorized into 3 components: 2 orthogonal matrices and 1 diagonal matrix.

$$A = USV^T \tag{3}$$

The SVD of matrix A is given by Eq. (3), where $U = [u_1, u_2, \dots u_m] \in R^{m \times m}$, $V = [v_1, v_2, \dots v_n] \in R^{n \times n}$, $S = diag(\sigma_1, \sigma_2, \sigma_3 \dots \sigma_p) \in R^{m \times n}$.

The singular values satisfy $\sigma_1 \geq \sigma_2 \geq \cdots \geq \sigma_p \geq 0$. The diagonal entries of S, i.e., σ_i are known as the singular values of A. The m columns of U are the left singular vectors and the n columns of V are the right singular vectors. SVD is a well-established technique in numerical linear algebra, primarily used for matrix analysis [14–16]. When applied to images, it provides 2 important advantages:

1. General applicability: unlike eigen decomposition, SVD is not limited to square matrices, thereby broadening the scope of possible decompositions.
2. Feature extraction: certain intrinsic or "inner fixed" features of the image can be derived from SVD. The inner features include singular values, left singular vectors, and right singular vectors. They are called "inner fixed" because they remain relatively stable under most image distortions and manipulations. Even geometric transformations, which often disrupt the spatial layout of pixels, do not significantly affect these features.

TABLE I. REVIEW OF RECENT WATERMARKING APPROACHES WITH THEIR KEY CONTRIBUTIONS AND LIMITATIONS

Ref.	Method	Optimization	Key Results	Limitations
[4]	LWT-DCT-SVD + Schur	Firefly	Dual watermarking, PSNR ≈ 45.8 dB, NCC = 1.0	No ML/encryption; lacks 3D/hardware focus
[5]	DWT-DCT-SVD, LWT-DCT-SVD	JAYA, PSO	JAYA > PSO, PSNR ≈ 44.9 dB, NCC = 1.0	Weak against histogram/motion blur; high complexity
[6]	LWT-DCT	PSO	PSNR ≈ 48 dB, NCC > 0.9; adaptive HVS region	Degrades under high noise/geometric attacks
[7]	RDWT-DCT-SVD	PSA	PSNR ≈ 73.7 dB, NCC ≈ 0.99998, robust overall	Grayscale only; high computational cost

Table I illustrates the techniques employed, contributions made, and limitations of selected watermarking methods documented in the literature.

III. PROPOSED METHOD

This research proposed a DWT-DCT-SVD Watermarking Using Cheetah Optimization Algorithm, the proposed watermarking framework consists of 2 main phases: embedding and extraction.

A. Embedding Phase

Fig. 3 illustrates the Embedding watermark. In the embedding stage, the host image undergoes a 2-level Discrete Wavelet Transform (DWT), followed by the application of the Discrete Cosine Transform (DCT) on the selected vertical detail sub-band. A central region of the DCT coefficients is then extracted and decomposed using Singular Value Decomposition (SVD). Similarly, the watermark image is processed using a single-level DWT, and SVD is applied to its vertical detail sub-band. Watermark information is embedded by modifying the singular values of the host image with those of the watermark, where the embedding strength is optimized using the Cheetah Optimization Algorithm to balance imperceptibility and robustness. Finally, inverse transformations (SVD, DCT, and DWT) are applied to reconstruct the watermarked image.

B. Extraction Phase

Fig. 4 illustrates the watermark extraction process. During extraction, the watermarked image undergoes the same sequence of transformations: 2-level DWT and DCT, followed by SVD on the central region. The watermark's singular values are recovered from the host's altered singular values using the known embedding strength. These recovered singular values are then combined with the original singular vectors of the watermark to reconstruct the watermark sub-band, and inverse DWT is applied to retrieve the final watermark image.

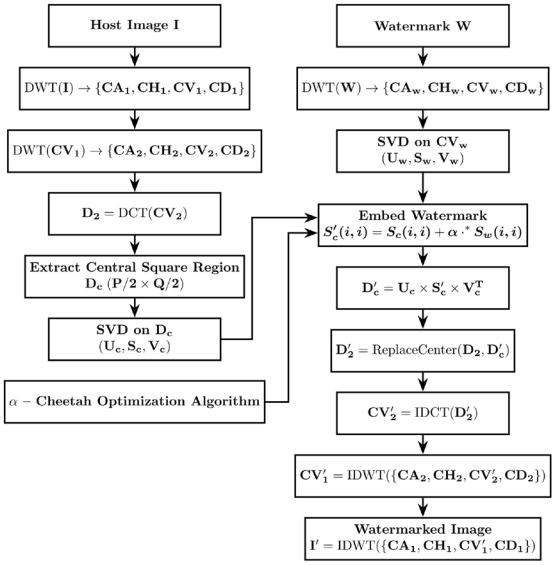

Fig. 3. Embedding watermark.

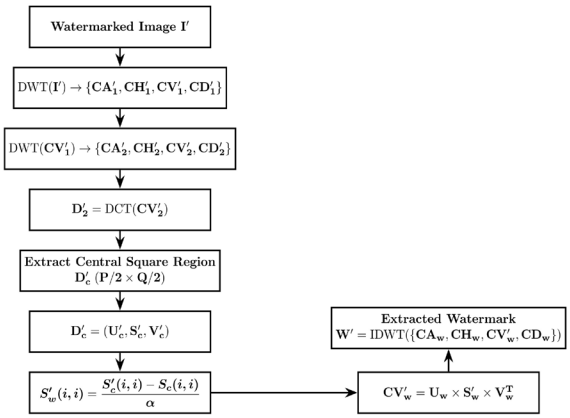

Fig. 4. Extracting watermark.

C. Watermark Embedding Algorithm

Table II presents the notations used to describe the watermarking methodology.

TABLE II. NOTATIONS USED IN THE PROPOSED WATERMARKING METHOD

Symbol	Meaning
I	Host image of size $M \times N$
W	Watermark image of size $P \times Q$
I'	Watermarked image
W'	Extracted watermark
α	Embedding strength factor (optimized by COA)
DWT	Discrete Wavelet Transform
IDWT	Inverse Discrete Wavelet Transform
DCT	Discrete Cosine Transform
IDCT	Inverse Discrete Cosine Transform
SVD	Singular Value Decomposition
CA, CH, CV, CD	Approximation, horizontal, vertical, diagonal coefficients
U, S, V	SVD components where $A = USV^T$

Algorithm 1 summarizes the watermark embedding process. The host image undergoes 2-level DWT followed by DCT and SVD on the CV sub-band, while the watermark image is processed using DWT and SVD. The watermark is embedded by modifying the singular values of the host image using an embedding strength optimized by the Cheetah Optimization Algorithm, and inverse transformations are applied to obtain the final watermarked image.

Algorithm 1: Watermark Embedding Algorithm

Input: Host image $I(M \times N)$, Watermark $W(P \times Q)$,
Output: Watermarked image $I'(M \times N)$

i. Apply 2-level DWT decomposition

$$\text{DWT}(I) \rightarrow \{CA_1, CH_1, CV_1, CD_1\}$$
$$\text{DWT}(CV_1) \rightarrow \{CA_2, CH_2, CV_2, CD_2\}$$

ii. Apply DWT on watermark

$$\text{DWT}(W) \rightarrow \{CA_W, CH_W, CV_W, CD_W\}$$

Retain $\{CA_W, CH_W, CD_W\}$

iii. Apply DCT on CV_2 sub-band

$$D_2 = \text{DCT}(CV_2)$$

iv. Extract central square region of D_2

The central region D_C should have dimensions equal to half the size of the watermark $(\frac{P}{2} \times \frac{Q}{2})$.

v. Apply SVD decomposition

$D_C = (U_C, S_C, V_C)$, $CV_W = (U_W, S_W, V_W)$

Retain S_C, U_W, V_W

vi. Embed watermark using modified singular values

$$S'_C(i,i) = S_C(i,i) + \alpha \times S_W(i,i)$$

for $i = 1$ to $(\frac{P}{2}$ or $\frac{Q}{2})$, α is determined by cheetah optimization algorithm.

vii. Reconstruct embedded coefficients

$$D'_C = U_C \times S'_C \times V_C^T$$

viii. Replace central region, apply inverse transforms

$D'_2 = \text{Replace center}(D_2, D'_C)$,

$CV'_2 = \text{IDCT}(D'_2)$,

$CV'_1 = \text{IDWT}(\{CA_2, CH_2, CV'_2, CD_2\})$,

$$I' = \text{IDWT}(\{CA_1, CH_1, CV'_1, CD_1\})$$

D. Watermark Extraction Algorithm

The watermark extraction follows an inverse sequence of operations used during embedding, beginning with multilevel decomposition and progressing to singular-value reconstruction. The complete procedure is outlined in Algorithm 2.

Algorithm 2: Watermark Extraction Algorithm

Input: Watermarked image $I'(M \times N)$, Original watermark size $P \times Q$, Output: Extracted watermark $W'(P \times Q)$

i. Apply 2-level DWT decomposition

$$\text{DWT}(I') \rightarrow \{CA'_1, CH'_1, CV'_1, CD'_1\},$$
$$\text{DWT}(CV'_1) \rightarrow \{CA'_2, CH'_2, CV'_2, CD'_2\}$$

ii. Apply DCT and extract central square region

$$D'_2 = \text{DCT}(CV'_2)$$

The central region D'_C should have dimensions equal to half the size of the watermark $\frac{P}{2} \times \frac{Q}{2}$.

iii. Apply SVD decomposition

$$D'_C = (U'_C, S'_C, V'_C)$$

iv. Extract watermark singular values

$$S'_W(i,i) = (S'_C(i,i) - S_C(i,i))/\alpha$$

for $i = 1$ to $(\frac{P}{2}$ or $\frac{Q}{2})$

v. Reconstruct watermark coefficients

$CV'_W = U_W \times S'_W \times V_W^T$,

$$W' = \text{IDWT}(\{CA_W, CH_W, CV'_W, CD_W\})$$

E. Cheetah Optimization Algorithm (COA)

Cheetahs (Acinonyx jubatus), the fastest land mammals, demonstrate exceptional hunting skills thanks to their rapid acceleration, agility, and short bursts of speed [17–19]. Their approach generally involves silent stalking to reduce detection, followed by a swift chase where agility and balance are used to corner prey. However, this burst of speed is energy-intensive and cannot be sustained for long, forcing the cheetah to succeed quickly or retreat. This balance between exploration (stalking and searching for prey) and exploitation (focused chase and capture) inspires the development of the Cheetah Optimization Algorithm (COA) [20]. Additionally, when unsuccessful, cheetahs return to their resting area, similar to a "return-to-home" strategy that prevents the algorithm from stagnating. The complete procedural steps of COA employed in this work are summarized in Algorithm 3. In the watermarking framework, COA is employed to find the optimal embedding strength (α) that balances robustness against attacks with the imperceptibility of the watermark.

In the proposed method, the CV sub-band was chosen for embedding due to its strong robustness features. The embedding process, summarized in Algorithm 1, is performed on the CV sub-band because experimental results showed that both the CV (vertical detail) and CH (horizontal detail) sub-bands consistently offered greater resistance to common image processing attacks compared to other sub-bands. By focusing on the CV sub-band, the scheme utilises this robustness while maintaining the perceptual quality of the watermarked image.

Furthermore, within the DCT domain, the central square region of the transformed coefficients was chosen for watermark embedding. This choice is driven by the fact that most mid-frequency components are concentrated in this region [10]. Mid-frequency coefficients strike an optimal balance between imperceptibility and robustness: they are less perceptible than low-frequency components, yet more resistant to common attacks than high-frequency components. Embedding in this region, therefore, improves the watermark's robustness while preserving the host image's high visual fidelity.

The image dimensions were also carefully chosen to balance imperceptibility and robustness effectively. Standard 512×512 grayscale images were used as host images, while the grayscale watermark size was fixed at 128×128. This configuration ensures that the watermark dimensions are one-quarter of the host image, a setup confirmed by experimental results to deliver optimal performance in terms of imperceptibility, robustness, and computational efficiency.

The proposed watermarking framework was initially designed to embed a single watermark, with the CV sub-band selected based on its experimentally demonstrated robustness. However, to enable a fair comparison with Awasthi *et al.* [4], which employs a dual-watermarking strategy, we extended our approach to embed 2 watermarks—one in the CV sub-band and another in the CH sub-band. This extension not only enables direct, balanced performance evaluation, but also demonstrates the adaptability of the proposed method to handle multiple watermarking scenarios without significant loss in imperceptibility or robustness. The corresponding watermark extraction procedure, which reverses the embedding operations, is summarized in Algorithm 2.

Algorithm 3: Cheetah Optimization Algorithm

Parameters:
M: Problem dimensionality
N: Population size
T: Current iteration (hunting time)
T_{max}: Maximum iterations (hunting time)
X_i: Position of cheetah ii
X_{best}: Global best position (prey)
X_{lead}: Leader position
X_{home}: Home position

Initialization

i. Initial population:

$$X_i = \text{rand}(M, N) \times (ub - lb) + lb$$

ii. Evaluate fitness $f(X_i)$ for all cheetahs

iii. Set $X_{best} = \text{argmaxf}(X_i)$

iv. Set $X_{lead} = X_{best}$

v. Set $X_{home} = \text{mean}(X_i)$

vi. Set $T = 0$

Main loop: **while** $T < T_{max}$

i. select a random subset of cheetahs

ii. **For** each selected cheetah *i*

For each dimension *j*
Generate random parameters
$\widehat{r_{i,j}} \sim N(0,1)$ (randomization factor)
$\widetilde{r_{i,j}} = |r|\, exp\left(\frac{r}{2}\right) sin(2\pi r)\,, r \sim N(0,1)$,
(turning factor)
$r_1, r_2 \sim U(0,1)$, $r_3 \sim U(0,1)$, $r_4 \sim U(0,3)$
step length: $\alpha_{i,j}^t = 0.001 \times (\frac{T}{T_{max}})$
Interaction factor: $\beta_{i,j}^t = X_{K,j}^t - X_{i,j}^t, K \neq i$

iii. choose hunting strategy

If $r_2 \geq r_3$
Sit and wait $X_{i,j}^{t+1} = X_{i,j}^t$
Else
Compute $H = e^{2\left(1-\frac{T}{T_{max}}\right)}(2r_1 - 1)$
If $H \geq r_4$
Attack $X_{i,j}^{t+1} = X_{B,j}^t + \widetilde{r_{i,j}} \times \beta_{i,j}^t$
Else
Search $X_{i,j}^{t+1} = X_{i,j}^t + \widetilde{r_{i,j}^{-1}} \times \alpha_{i,j}^t$

iv. update leader and best (for maximization)

If $f\left(X_i^{t+1}\right) > f(X_{lead}^t)$: $X_{lead}^{t+1} = X_i^{t+1}$
If $f\left(X_{lead}^{t+1}\right) > f(X_{best}^t)$: $X_{best}^{t+1} = X_{lead}^{t+1}$

v. leave prey and go back home:

If leader position is unchanged for a while:
$X_{lead} = X_{home}$, $X_{home} = \text{mean}(X_i)$
Reset $T = 0$

vi. Increment Iteration

$T = T + 1$

Final solution $X_{best} =$ maximum of the objective function.
Output: Optimal embedding strength $\alpha = X_{best}$

Compared with recent watermarking approaches, the proposed DWT–DCT–SVD method optimized using the Cheetah Optimization Algorithm (COA) stands out in several respects. Unlike previous research rely on complex hybrids such as LWT, RDWT, Schur decomposition, or triple-level transforms [4–7], our method strategically embeds in the CV sub-band and central DCT region, offering a balanced trade-off between imperceptibility and robustness. While existing works employ Firefly, JAYA, PSO, or Porcellio Scaber algorithms for optimization, COA introduces a novel, less-explored bio-inspired strategy with effective exploration–exploitation balance. Security in prior studies often depends on external mechanisms such as Speeded-Up Robust Features (SURF) authentication or chaotic encryption. In contrast, our approach emphasizes robustness through optimized embedding and naturally extends to dual watermarking for fair comparison with previous method posed by Awasthi *et al.* [4]. In terms of complexity, the proposed framework is more straightforward and computationally more efficient than multi-transform or multi-optimization schemes, yet it achieves competitive performance. Overall, the method combines targeted mid-frequency embedding, flexible watermark capacity (single or dual), and COA-based optimization to deliver a practical balance of imperceptibility, robustness, and efficiency that sets it apart from earlier approaches.

IV. Results and Discussion

This research assesses 2 core aspects of digital image watermarking: imperceptibility and robustness. Standard test images, such as Lena, Baboon, and Cameraman, are used as host images, while various logos serve as watermarks.

Figs. 5 and 6 illustrate the set of host images and watermarks employed in the proposed method. The evaluation depends on 3 standard performance metrics: PSNR and Structural Similarity Index Measure (SSIM) for imperceptibility, and Normalized Cross Correlation (NCC) for robustness.

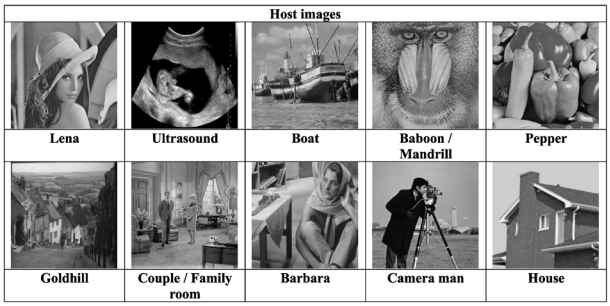

Fig. 5. Set of Host images used for watermark embedding.

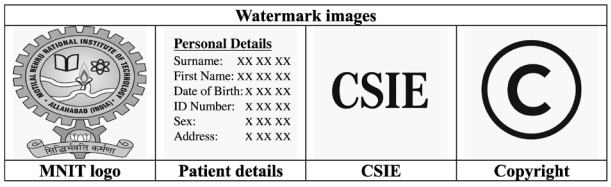

Fig. 6. Watermark images used in proposed method.

Illustrative results of the proposed watermarking scheme under different attacks are presented in Fig. 7, which includes noise-based distortions and common filtering operations applied to the host and watermark images from Ref. [4].

Additional attack scenarios, including both noise and enhancement-based distortions using images from Ref. [5], are shown in Fig. 8. Further results demonstrating the method's behavior under noise, filtering, and enhancement attacks with images from Ref. [6] are provided in Fig. 9. Extended evaluations using images from Ref. [7], covering geometric attacks such as rotation and scaling along with histogram and filtering operations, are displayed in Fig. 10. Each figure displays the attacked watermarked images alongside the corresponding extracted watermarks. For evaluation, host images and watermarks were sourced from the literature that this study aims to compare against.

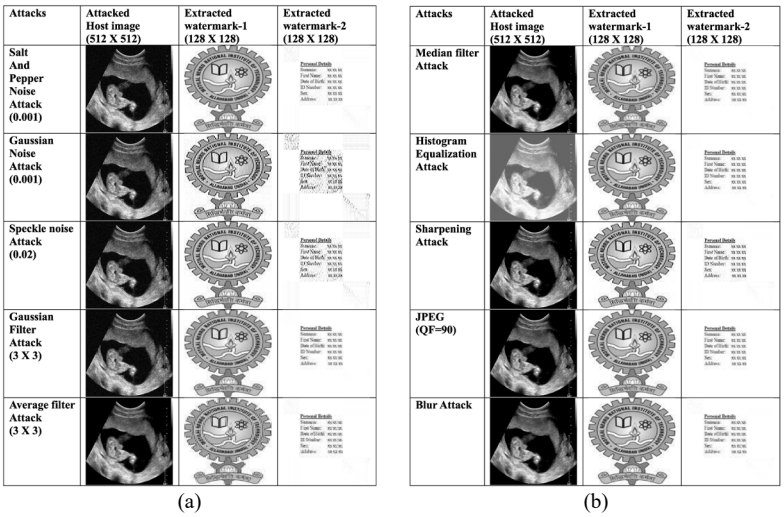

Fig. 7. Watermarked images and extracted watermarks under attacks, host and watermark images from Ref. [4]. (a) Salt and pepper, gaussian, speckle, gaussian filter and average filter. (b) Median filter, histogram equalization, sharpening, JPEG, blur.

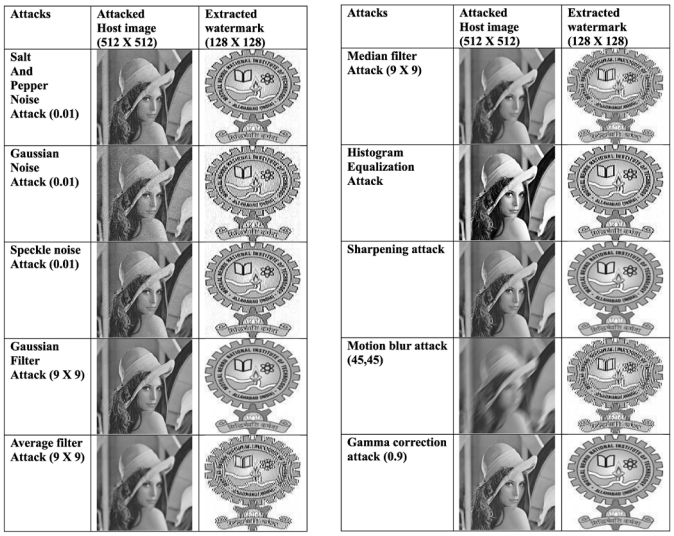

(a) (b)

Fig. 8. Watermarked images and extracted watermarks under attacks, host and watermark images from Ref. [5]. (a) Salt and pepper, gaussian, speckle, gaussian filter, average filter. (b) Median filter, histogram equalization, sharpening, motion blur, gamma correction.

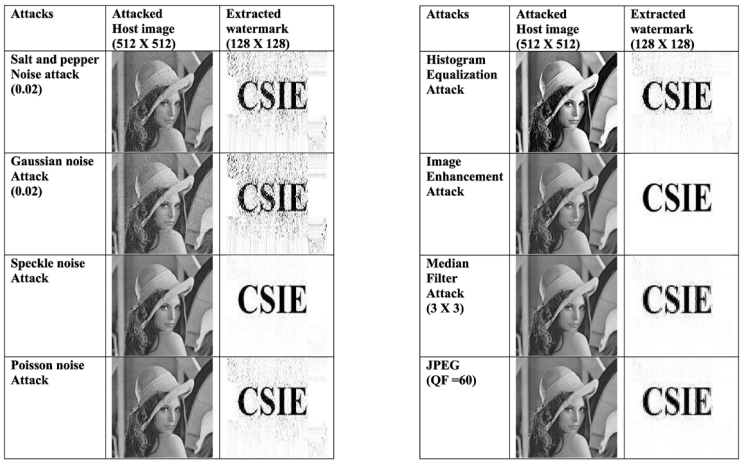

(a) (b)

Fig. 9. Watermarked images and extracted watermarks under attacks, host and watermark images from Ref. [6]. (a) Salt and pepper, gaussian, speckle, Poisson. (b) Histogram equalization, image enhancement, median filter, JPEG.

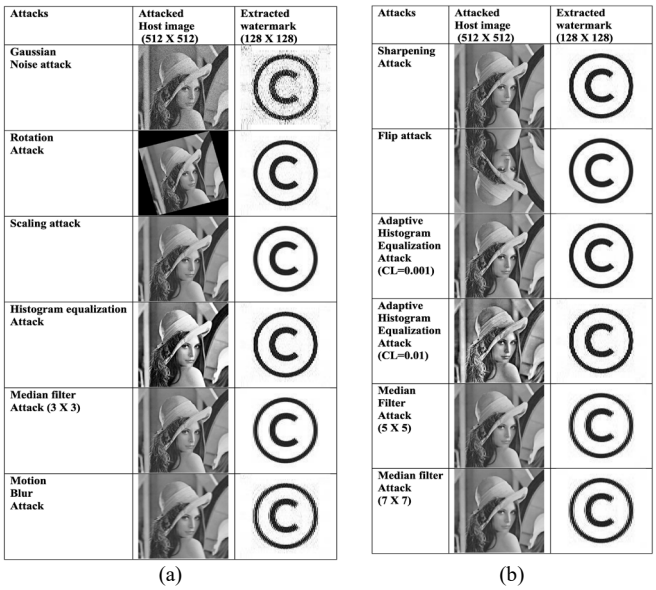

(a) (b)

Fig. 10. Watermarked images and extracted watermarks under attacks, host and watermark images from Ref. [7]. (a) Gaussian, rotation, scaling, histogram equalization, median filter, motion blur. (b) Sharpening, flip, adaptive histogram equalization, median filter.

Table III shows the Input Datasets for Host and Watermark Images for the Existing Methods and the Proposed Method. In our study, both the host and watermark images are grayscale and designed to be square (equal length and width). This choice aligns with common practice in digital watermarking research, where standard benchmark images (e.g., Lena, Baboon, Cameraman) are usually of square dimensions, allowing for fair comparison with previous studies. Furthermore, a square watermark facilitates balanced embedding across sub-bands and simplifies transform-domain processing. Although rectangular images were not considered here, exploring such cases remains a promising area for future research.

TABLE III. INPUT DATASETS OF HOST AND WATERMARK IMAGES FOR EXISTING METHODS AND PROPOSED METHOD

Ref. No	Host Images	Host Image Size	Watermark Images	Watermark Size
[4]	DICOM Ultrasound liver images (3 patients) from Cancer Imaging Archive	512 × 512	(1) MNNIT logo, (2) Patient details	256 × 256 each
[5]	Standard grayscale images: Lena, Boat, Baboon, Pepper, Goldhill, Couple, X-ray lungs, MRI	512 × 512	Motilal Nehru National Institute of Technology (MNNIT) logo	256 × 256
[6]	Standard grayscale images: Lena, Cameraman, House, Mandrill, Barbara, Alain, Einstein, Family room, Boat, Peppers, Jet Plane	512 × 512	Binary logos: National Institute of Technology (NIT) Silchar, Computer Science and Information Engineering (CSIE)	32 × 32
[7]	Standard grayscale images: Lena, Cameraman, Baboon, Barbara, Peppers, Boat	Not mentioned	Copyright logo	Not mentioned
Proposed Method	Standard grayscale images: DICOM Ultrasound liver image, Lena, Boat, Baboon, Pepper, Goldhill, Couple, Cameraman, House, Barbara	512 × 512	MNNIT logo, Patient details, CSIE, Copyright logo	128 × 128

- Peak Signal to Noise Ratio (PSNR)

PSNR is the ratio between the maximum power of a signal to the maximum power of Noise signal [21–23]. PSNR is a widely used objective measure that compares the similarity between the original image and the watermarked (or distorted) image. It is derived from the Mean Squared Error (MSE) as defined in Eq. (4) and expressed in decibels (dB). MSE is defined in Eq. (5). If $x(i,j)$ is the original reference image and $y(i,j)$ is the distorted image, then the Peak Signal to Noise Ratio (PSNR) is given by Eqs. (4) and (5)

$$PSNR = 10log_{10}\frac{L^2}{MSE} \tag{4}$$

$$MSE = \frac{1}{MN}\sum_{i=0}^{M-1}\sum_{j=0}^{N-1}[x(i,j) - y(i,j)]^2 \tag{5}$$

where M and N are dimensions of the image. L is the dynamic range of the image pixels. Higher value of PSNR means a good value. PSNR is an excellent measure of quality for white noise distortion. PSNR involves simple calculations, has clear physical meaning and is convenient in context of optimization but PSNR is not according to the characteristics of Human Visual System (HVS).

To quantify the similarity between 2 images, correlation-based measures are adopted. 2 different forms of Normalized Cross Correlation are used in this work.

- Normalized Cross Correlation (NCC)

Two commonly used forms of NCC are defined in Eqs. (6) and (7). The normalized cross correlation is defined as Eq. (6) [6, 7]:

$$NCC = \frac{\sum_{i=0}^{M-1}\sum_{j=0}^{N-1}x(i,j)y(i,j)}{\sum_{i=0}^{M-1}\sum_{j=0}^{N-1}(x(i,j))^2} \tag{6}$$

where $x(i,j)$ represents the reference image and $y(i,j)$ denotes the test image. This definition normalizes with respect to the reference image only and hence is asymmetric. Although simpler, it provides a useful measure when one image is treated as the ground truth.

To evaluate robustness more rigorously, the standard normalized cross correlation is also employed, which is defined as Eq. (7) [4, 5]:

$$NCC = \frac{\sum_{i=0}^{M-1}\sum_{j=0}^{N-1}x(i,j)y(i,j)}{\sqrt{\sum_{i=0}^{M-1}\sum_{j=0}^{N-1}x^2(i,j)}\sqrt{\sum_{i=0}^{M-1}\sum_{j=0}^{N-1}y^2(i,j)}} \tag{7}$$

where $x(i,j)$ and $y(i,j)$ denote the original and recovered watermarks respectively, and $x^2(i,j)$, $y^2(i,j)$ represent their squared pixel values. This measure is symmetric and bounded in the range [−1,1], making it widely adopted in watermarking literature.

- Structural Similarity Index Measure (SSIM)

SSIM is a Human Visual System (HVS) feature-based metric proposed by Wang *et al.* [24]. SSIM measures the similarity between 2 images [25]. It is an improvement over methods like MSE and PSNR. It is calculated over several windows of image as Eq. (8):

$$SSIM(x,y) = \frac{(2\mu_x\mu_y + C_1)(2\sigma_{xy} + C_2)}{(\mu_x^2 + \mu_y^2 + C_1)(\sigma_x^2 + \sigma_y^2 + C_2)} \tag{8}$$

where μ_x and μ_y are the average of x and y respectively, σ_x^2 and σ_y^2 are the variance of x and y respectively, σ_{xy} is the covariance of x and y, constraints $C_1 = (K_1L)^2$ and $C_2 = (K_2L)^2$, L = Dynamic range of pixel values = 255, $K_1 = 0.01$ and $K_2 = 0.03$.

The proposed watermarking technique underwent a comprehensive comparative analysis against 4 established methods from the reference.

- Robust, imperceptible and optimized watermarking of Digital Imaging and Communications in Medicine (DICOM) image using Schur decomposition, LWT-DCT-SVD and its authentication using SURF [4].
- LWT-DCT-SVD and DWT-DCT-SVD based watermarking schemes with their performance enhancement using Jaya and Particle swarm

optimization and comparison of results under various attacks [5].

- A robust digital image watermarking technique in LWT-DCT domain using particle swarm optimization and statistical distortion correction [6].
- An Optimized Hybrid Algorithm for Blind Watermarking Scheme Using Singular Value Decomposition in RDWT-DCT Domain [7].

Across various references, a range of robustness tests were performed to assess watermarking performance under attacks. Awasthi *et al.* [4] examined noise attacks such as salt and pepper, Gaussian, and speckle noise, as well as filtering attacks including Gaussian low-pass, average, and median filters, along with histogram equalization, sharpening, JPEG compression, and motion blur. Awasthi *et al.* [5] applying similar noise and filtering attacks but with larger filter sizes, and additionally included gamma correction. Barlaskar *et al.* [6] tested a broader set of distortions, including salt and pepper, Gaussian, speckle, and Poisson noise, histogram equalization, image enhancement, median filtering, and JPEG compression. Rajani *et al.* [7] focused on both non-geometric and geometric attacks, covering Gaussian noise, rotation, scaling, flipping, histogram equalization, adaptive histogram equalization with various clip limits, median filtering with different window sizes, motion blur, and sharpening. To evaluate the robustness of the proposed method, watermark resilience was tested against a wide range of image processing and geometric attacks, including noise addition in the form of salt-and-pepper, Gaussian, speckle, and Poisson noise [26], filtering operations such as Gaussian low-pass and median filtering along with histogram equalization [27], and transformations like motion blur, enhancement, and sharpening [28]. Additional attacks tested were geometric operations including rotation and flipping [29], JPEG compression [30], average filtering [31], and gamma correction [32]. The simulations were conducted using MATLAB 2018 software. The parameters for determining the embedding factors—including iteration count and population size for the COA—remained consistent across all comparisons. A population size of 10 and 10 iterations were utilised. COA was employed to find the optimal embedding factor that improves the fitness function, which aims to maximise the PSNR of the watermarked image and NCC of the extracted watermark under both no-attack and attacked conditions, as defined in Eq. (9).

$$fitness = PSNR_{wkd} + NCC_{ewk} + \sum_{i=1}^{N} NCC_{ewka}(i) \quad (9)$$

where PSNR_{wkd} is the PSNR of the watermarked image, NCC_{ewk} is the NCC of the extracted watermark under no attack, and $\mathrm{NCC}_{ewka}(i)$ is the NCC of the extracted watermark under the i^{th} attack. N is the total number of attacks considered.

A. Imperceptibility Analysis

Table IV presents the no-attack performance comparison between Ref. [4] and the proposed method using the ultrasound image, the proposed approach achieved a PSNR of 49.4417 dB on the Ultrasound host image, surpassing the 45.8168 dB obtained by Ref. [4], indicating an 8% improvement. The SSIM values remained above 0.9950, confirming excellent imperceptibility in medical DICOM contexts.

Table V summarizes the no-attack comparison with Ref. [5] across 6 standard images. For Ref. [5] (DWT-DCT-SVD using the Jaya optimization algorithm), the PSNR values for the watermarked images ranged from 42.3417 dB (Baboon) to 44.9488 dB (Lena) across the test images (Lena, Boat, Baboon, Pepper, Goldhill, Couple). In contrast, the proposed method consistently achieved PSNR values above 55 dB for all images, representing an improvement of approximately 24–30%, shows notable improvements achieved by the proposed method.

Table VI presents a comprehensive no-attack comparison with Ref. [6] for 7 benchmark images, the results show a clear improvement in image quality. The PSNR values in Ref. [6] ranged from 43.61 dB (Barbara) to 52.29 dB (Lena), while the SSIM values varied from 0.8899 (Family Room) to 0.9991 (House), with noticeable quality reduction in complex images such as Mandrill (45.59 dB, SSIM = 0.9329). In comparison, the proposed method achieved nearly uniform PSNR values around 57 dB for all test images and consistently high SSIM values above 0.9986, demonstrating significant improvements in both imperceptibility and structural similarity, with overall PSNR gains of 9–31%.

TABLE IV. COMPARISON OF METRICS FOR REF. [4] AND PROPOSED METHOD IN NO-ATTACK CASE

Host image	Watermarked Image No Attack		Extracted Watermarks No Attack	
	PSNR (dB)	SSIM	Watermark-1 NCC	Watermark-2 NCC
P1-ultrasound [4]	45.8168	0.9969	1.0000	1.0000
Ultrasound (proposed method)	49.4417	0.9954	0.9999	1.0000

TABLE V. COMPARISON OF METRICS FOR REF. [5] AND PROPOSED METHOD IN NO-ATTACK CASE

Input Images	Lena	Boat	Baboon	Pepper	Goldhill	Couple
PSNR Watermarked Image [5]	44.9488	44.3973	42.3417	43.2800	44.6008	44.5323
NCC Extracted Watermark [5]	1.0000	1.0000	1.0000	1.0000	1.0000	1.0000
PSNR Watermarked Image (Proposed method)	55.2726	55.2178	55.0129	55.2648	55.0545	55.2839
NCC Extracted Watermark (Proposed method)	1.0000	1.0000	1.0000	1.0000	1.0000	1.0000

TABLE VI. COMPARISON OF METRICS FOR REF. [6] AND PROPOSED METHOD IN NO-ATTACK CASE

Input Images	Lena	Cameraman	House	Mandrill	Barbara	Family Room	Boat
PSNR Watermarked [6]	52.29	49.89	51.06	45.59	43.61	46.67	48.31
SSIM Watermarked [6]	0.9934	0.9677	0.9991	0.9329	0.9812	0.8899	0.9919
NCC Extracted [6]	1.000	0.9773	0.9990	0.9439	0.9990	0.9838	0.9992
PSNR Watermarked (Proposed method)	57.1744	57.2273	57.3862	57.4375	57.3569	57.2854	57.1580
SSIM Watermarked (Proposed method)	0.9989	0.9989	0.9988	0.9986	0.9989	0.9988	0.9988
NCC Extracted (Proposed method)	0.9988	0.9991	0.9985	0.9981	0.9987	0.9985	0.9981

Finally, Table VII compares the IQA metrics of the watermarked Lena image between Ref. [7] and the proposed method, the proposed method underperformed the RDWT-DCT-SVD approach, which achieved an exceptionally high PSNR of 73.72 dB, compared with 57.79 dB for the Proposed Method, representing a 21.6% difference. Despite this isolated case of underperformance, the PSNR obtained by the Proposed method still remains within the high-quality imperceptibility range, indicating visually negligible distortion.

TABLE VII. COMPARISON OF IQA METRICS OF THE WATERMARKED IMAGE FOR REF. [7] AND PROPOSED METHOD IN NO-ATTACK CASE

IQA Metrics	Ref. [7]	Proposed Method
PSNR-Lena	73.72	57.79

Overall, the imperceptibility analysis confirms that the Proposed Method consistently achieves superior or comparable performance to existing methods across most datasets, with a notable exception only in Table VII.

B. Robustness Analysis

Normalized Cross-Correlation (NCC) values under no-attack conditions indicate the accuracy of watermark recovery when no distortions are present. Ideally, NCC should be 1.0000, signifying perfect similarity between the original and extracted watermark.

From Table IV, both Ref. [4] and the proposed method achieve near-perfect NCC values (≥ 0.9999) for dual watermark embedding, demonstrating that watermark information is preserved intact. Similarly, in Table V, both Ref. [5] and the proposed approach report NCC = 1.0000 across all test images, confirming flawless watermark extraction.

In Table VI, Ref. [6] achieves high NCC values, but slight deviations (e.g., 0.9773 for Cameraman and 0.9439 for Mandrill) indicate minor distortions during extraction. In contrast, the proposed method consistently maintains NCC values very close to unity ($\geq$0.9981), ensuring highly reliable watermark recovery.

Overall, the results confirm that the proposed method achieves precise watermark extraction under no-attack conditions, matching or exceeding existing techniques, with NCC values consistently close to 1.0000.

The robustness evaluation further emphasizes the Proposed Method's resistance to diverse image processing and geometric attacks. Table VIII provides a robustness comparison between Ref. [4] and the proposed method under various signal-processing attacks, for Watermark-1, both Ref. [4] and the Proposed Method achieved high correlation values under all attack conditions, indicating strong robustness. The Proposed Method maintained perfect correlation under Salt and Pepper noise (1.0000) and slightly lower performance than Ref. [4] under Gaussian noise (0.9929 vs. 0.9995) and Average filtering (0.9918 vs. 0.9957). However, it achieved higher NCC under Speckle noise (0.9985 vs. 0.9971), Histogram Equalization (0.9997 vs. 0.9845), Sharpening (0.9978 vs. 0.9730), and Motion Blur (0.9995 vs. 0.9982).

TABLE VIII. COMPARATIVE ROBUSTNESS ANALYSIS OF EXTRACTED WATERMARKS BETWEEN REF. [4] AND PROPOSED METHOD

Attacks	Watermark-1 [4] NCC	Watermark-2 [4] NCC	Watermark-1 NCC (Proposed method)	Watermark-2 NCC (Proposed method)
Salt and Pepper (0.001)	0.9998	0.9999	1.0000	1.0000
Gaussian Noise (0.001)	0.9995	0.9994	0.9929	0.9999
Speckle Noise (0.02)	0.9971	0.9984	0.9985	0.9947
Gaussian Low Pass Filter (3 × 3)	0.9995	0.9998	0.9984	0.9985
Average Filter (3 × 3)	0.9957	0.9981	0.9918	0.9997
Median Filter (3 × 3)	0.9997	0.9999	0.9957	0.9986
Histogram Equalization	0.9845	0.9861	0.9997	0.9994
Sharpening	0.9730	0.9876	0.9978	0.9999
JPEG (90)	0.9994	0.9998	0.9995	0.9996
Motion Blur	0.9982	0.9921	0.9995	0.9998

For Watermark-2, both methods also performed comparably, with NCC values close to unity in all cases. The Proposed Method achieved the same or slightly better results under Salt and Pepper (1.0000 vs. 0.9999), Gaussian noise (0.9999 vs. 0.9994), Average filtering (0.9997 vs. 0.9981), and Sharpening (0.9999 vs. 0.9876). In a few cases, such as Speckle noise (0.9947 vs. 0.9984) and Gaussian low-pass filtering (0.9985 vs. 0.9998), the baseline performed marginally better. Overall, NCC values indicate that the Proposed Method and Ref. [4] exhibit similar robustness characteristics, with the Proposed Method showing noticeable improvement particularly under Histogram Equalization and Sharpening attacks.

Table IX compares the robustness of the proposed method against several prior DWT-DCT-SVD and LWT-DCT-SVD watermarking variants from Ref. [5], the Proposed Method consistently demonstrates robustness

across various attacks. Against Histogram Equalization, where all baseline approaches collapsed to ≈0.72 NCC, the Proposed Method achieved 0.9902, reflecting a 37% improvement. Similarly, in Sharpening, the Proposed Method attained 1.0000 NCC compared to ≈0.991 for baseline schemes. Although slightly less effective under Gaussian noise (0.9733) compared to other schemes (>0.997), and somewhat reduced in Median Filtering (0.9695), the Proposed Method maintains strong overall robustness, with notable advantages in several challenging scenarios.

TABLE IX. COMPARATIVE ROBUSTNESS ANALYSIS OF EXTRACTED WATERMARKS BETWEEN REF. [5] AND PROPOSED METHOD

Attacks	NCC Values				
	DWT-DCT-SVD With PSO	DWT-DCT-SVD With Jaya	LWT-DCT-SVD With PSO	LWT-DCT-SVD With Jaya	Proposed Method
Salt and Pepper (0.01)	0.9807	0.9696	0.9976	0.9719	0.9926
Gaussian noise (0.01)	0.9983	0.9976	0.9981	0.9977	0.9733
Speckle noise (0.01)	0.9917	0.9925	0.9956	0.9905	0.9929
Gaussian low pass filter (9 × 9)	0.9996	0.9961	0.9996	0.9961	1.0000
Average Filter (9 × 9)	0.9622	0.9512	0.9622	0.9512	0.9542
Median Filter (9 × 9)	0.9966	0.9958	0.9966	0.9958	0.9695
Histogram Equalization	0.7183	0.7213	0.7183	0.7213	0.9902
Sharpening	0.9915	0.9904	0.9915	0.9904	1.0000
Motion Blur (45, 45)	0.8932	0.8820	0.8932	0.8820	0.9594
Gamma Correction 0.9	0.9874	0.9871	0.9874	0.9871	0.9999

Table X reports the robustness comparison with Ref. [6] under a range of degradations such as noise, filtering, Poisson noise, histogram equalization, image enhancement, JPEG compression, and speckle noise, the proposed method consistently outperformed the LWT-DCT-PSO approach, achieving notable improvements under most attack scenarios. For instance, NCC increased from 0.9370 to 0.9926 under Speckle noise and from 0.9291 to 0.9792 under Histogram Equalization. Filtering attacks also demonstrated significant enhancements, with Median Filtering (0.9876 vs. 0.9506) and JPEG compression (0.9876 vs. 0.9344) emphasizing the robustness of the Proposed Method. A slight decrease was only observed with Gaussian noise (0.9215 vs. 0.9488), indicating a trade-off under substantial additive noise.

TABLE X. COMPARATIVE ROBUSTNESS ANALYSIS OF EXTRACTED WATERMARKS BETWEEN REF. [6] AND PROPOSED METHOD

Attacks	NCC values	
	LWT-DCT With PSO [6]	Proposed Method
Salt and Pepper (0.02)	0.9546	0.9410
Gaussian noise (0.02)	0.9488	0.9215
Speckle noise	0.9370	0.9926
Poisson noise	0.9746	0.9706
Histogram Equalization	0.9291	0.9792
Image Enhancement	0.9681	0.9989
Median Filter (3 × 3)	0.9506	0.9876
JPEG (Q = 60)	0.9344	0.9876

Finally, Table XI compares robustness with Ref. [7] across diverse attacks such as rotation, scaling, histogram equalization, adaptive histogram equalization, median filtering, motion blur, sharpening, and flipping, the Proposed Method demonstrated superior performance under most attacks. Against Rotation, the Proposed Method recorded a 0.9894 NCC, significantly higher than 0.9179, representing a 7.8% improvement. Similarly, for Motion Blur, the Proposed Method increased from 0.9345 to 0.9897 (a 5.9% gain). However, marginal decreases were noted in Gaussian Noise (0.9371 vs. 0.9762) and Sharpening (0.9913 vs. 0.9935), indicating that noise-dominant distortions remain more challenging. Finally, in the no-attack case, both Ref. [7] (0.9999) and the proposed method (0.9984) yield nearly identical performance, with negligible differences.

TABLE XI. COMPARATIVE ROBUSTNESS ANALYSIS OF EXTRACTED WATERMARKS BETWEEN REF. [7] AND PROPOSED METHOD

Attacks	NCC [7]	NCC Proposed Method
No Attack	0.9999	0.9984
Gaussian Noise	0.9762	0.9371
Rotation	0.9179	0.9894
Scaling	0.9922	0.9962
Histogram Equalization	0.9742	0.9879
Adaptive Histogram Equalization (CL = 0.001)	0.9972	0.9966
Adaptive Histogram Equalization (CL = 0.01)	0.9714	0.9867
Median Filter (3 × 3)	0.9944	0.9925
Median Filter (5 × 5)	0.9784	0.9872
Median Filter (7 × 7)	0.9610	0.9838
Motion Blur	0.9345	0.9897
Sharpening	0.9935	0.9913
Flipping	0.9999	0.9984

Overall, the robustness analysis shows that the Proposed Method delivers superior performance in most attack scenarios across comparisons, particularly in geometric distortions (Rotation, Scaling) and enhancement-based attacks (Histogram Equalization, Sharpening), with only minor weaknesses against Gaussian noise.

Fig. 11 illustrates the comparative evaluation of Image Quality Assessment (IQA) metrics for watermarked images under no-attack conditions, corresponding to the Tables IV–VII. Fig. 11(a) presents the PSNR and SSIM performance for the ultrasound image, Fig. 11(b) compares PSNR values across standard test images, Fig. 11(c) reports PSNR results for additional benchmark images, Fig. 11(d) depicts SSIM comparisons, and Fig. 11(e) highlights the PSNR performance of the proposed method against an existing method for the Lena image.

Fig. 12 shows the NCC comparison of extracted watermarks from ultrasound and standard images under no-attack conditions for both reference and proposed methods. Fig. 12(a) presents the NCC values obtained from ultrasound images, Fig. 12(b) and Fig. 12(c) display the NCC results for standard test images. Fig. 13 shows the NCC-based comparison of extracted watermarks under various signal processing and geometric attacks. Fig. 13 (a)–(d) present the NCC values obtained under different attack scenarios for the proposed method and existing methods.

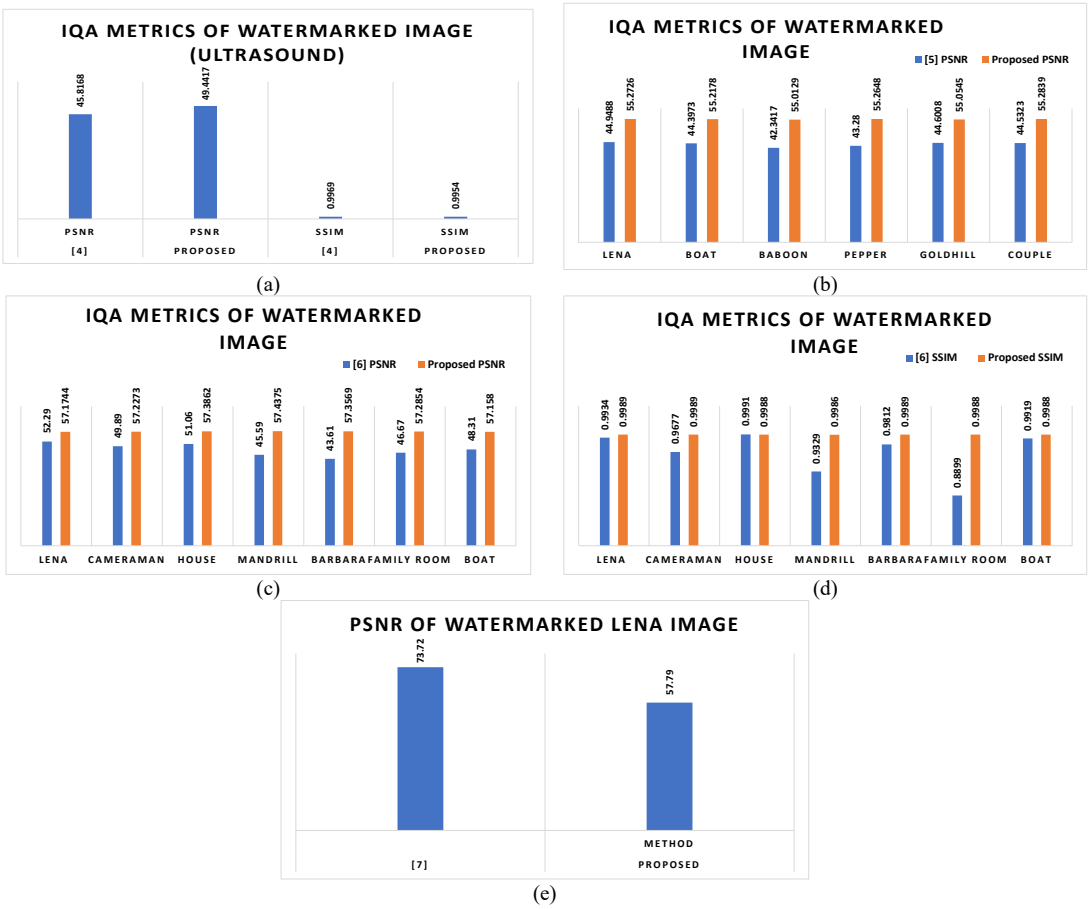

Fig. 11. Image quality assessment of watermarked images without attacks. (a) Ultrasound PSNR, SSIM. (b) PSNR compared with Ref. [5]. (c) PSNR compared with Ref. [6]. (d) SSIM. (e) PSNR compared with Ref. [7]. (Lena) Subfigures (b-d) correspond to standard test images.

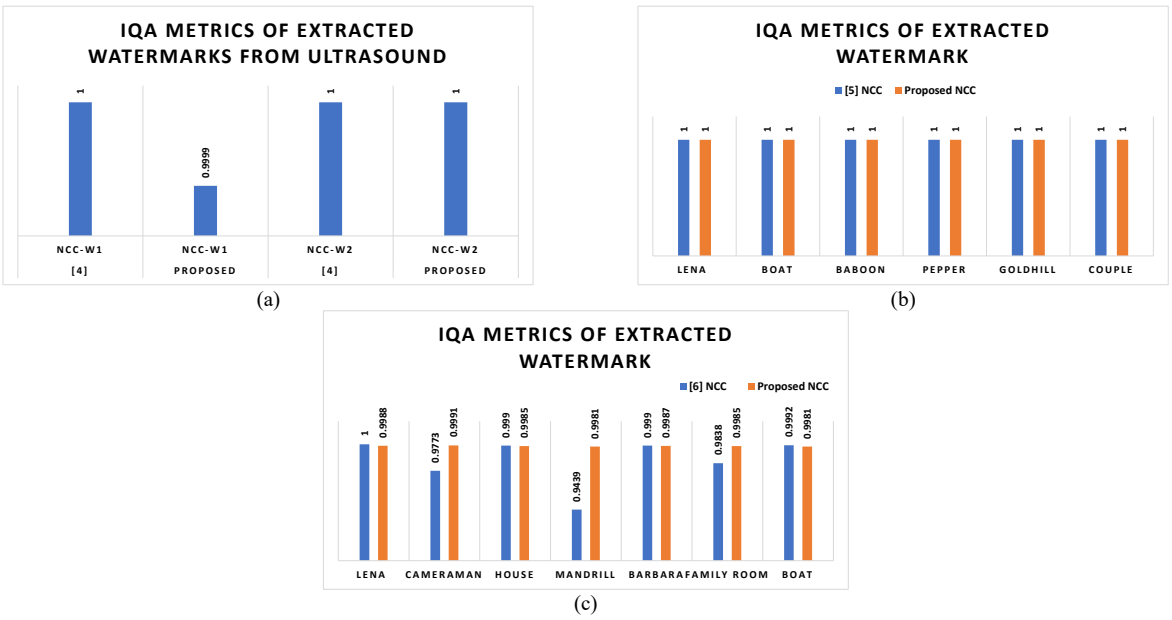

Fig. 12. NCC comparison of extracted watermarks from ultrasound and standard images under no-attack conditions for reference and proposed methods. (a) Ultrasound. (b) Standard images compared with Ref. [5]. (c) Standard images compared with Ref. [6].

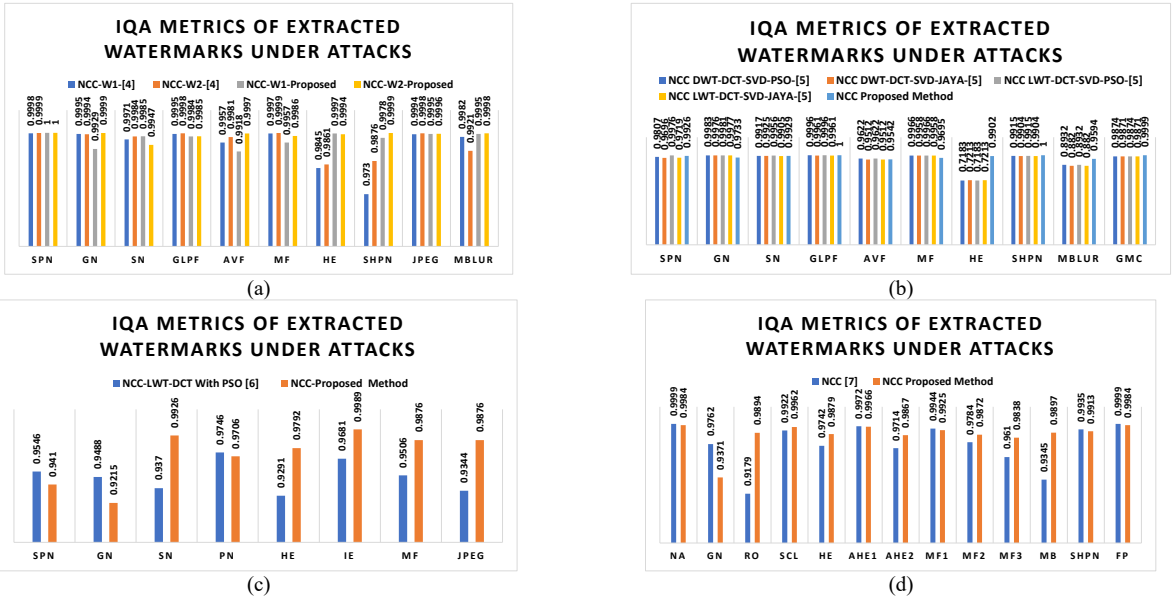

Fig. 13. NCC-based robustness comparison of extracted watermarks under various attacks with existing methods. (a) Noise and filtering attacks; (b) Noise, filtering, and intensity adjustment attacks; (c) noise, enhancement, and compression attacks; (d) Noise, filtering, intensity, and geometric attacks.

The evaluated attacks in Figs. 12 and 13 include: NCC-W1/NCC-W2-NCC of watermark 1/watermark 2, SPN-Salt and pepper noise, Gaussian Noise (GN), Speckle Noise (SN), Poisson Noise (PN), Gaussian Low Pass Filter (GLPF), Average Filter (AVF), Histogram Equalization (HE), Sharpen (SHPN), Motion Blur (MBLUR/MB), Gamma Correction (GMC), Image Enhancement (IE), Rotation (RO), Scaling (SCL), Flip (FP).

C. Watermark Capacity Rate

The watermark capacity rate is measured in bits per pixel (bpp), representing the ratio of the number of embedded watermark bits to the total number of pixels in the host image. Watermark capacity rate (also referred to as payload capacity or embedding capacity) indicates how much watermark data can be embedded into the host image without significantly compromising its quality [33–35]. The common formula is:

$$capacity\ rate\ (bits\ per\ pixel, bpp) = \frac{No\ of\ watermark\ bits\ embedded}{total\ number\ of\ pixels\ in\ host\ image}$$

If the host image size is $M \times N$, then total pixels $= MN$. If watermark size $= P \times Q$, then total watermark bits $= PQ$ (for binary watermark). For gray watermarks, the bit-depth also matters (8 bit gray scale) $= 8PQ$.

$$capacity\ rate\ (bits\ per\ pixel, bpp) = \frac{8PQ}{MN}$$

The watermarking capacity values for different methods are summarized in Table XII. It is clear that earlier works achieved significantly higher embedding capacities (2.00 and 4.00 bpp, respectively) by using relatively larger watermark sizes [4, 5]. In contrast, the proposed method intentionally maintains a lower watermarking capacity (0.50 bpp for a single 128×128 watermark and 1.00 bpp when embedding 2 watermarks). This design choice is deliberate, as the proposed framework focuses not on maximizing payload but on balancing imperceptibility, robustness, and hardware feasibility. By keeping the watermark size moderate, the computational complexity and memory requirements are substantially reduced. This is especially important because the ultimate aim of this research is to implement the algorithm on FPGA and ASIC platforms, where hardware resources, power consumption, and processing speed impose strict constraints. Thus, while the payload capacity of the proposed approach is lower than that of some previous works, this trade-off is justified by the need for an efficient, practical hardware implementation without compromising imperceptibility and robustness.

TABLE XII. WATERMARK PAYLOAD CAPACITY (BPP) OF EXISTING AND PROPOSED SCHEMES

Reference Number	Host Image	Watermark Image	Watermark Bits	Host Pixels	Watermark Capacity
[4]	512 × 512	256 × 256	524,288	262,144	2.00
[5]	512 × 512	2 × 256 × 256	1,048,576	262,144	4.00
[6]	512 × 512	32 × 32	1024	262,144	0.003
Proposed Method	512 × 512	128 × 128	131,072	262,144	0.50
Proposed Method	512 × 512	2 × 128 × 128	262,144	262,144	1.00

D. Computational Cost

Computation time, also known as execution time, refers to the total duration an algorithm takes to complete all its operations from start to finish [36, 37]. In digital image watermarking, it indicates the interval between beginning the watermark embedding or extraction process and receiving the final watermarked image or extracted

watermark. It is typically measured in seconds or milliseconds and serves as a key performance indicator for evaluating the algorithm's efficiency. Table XIII presents the computational time analysis for watermark embedding and extraction across different methods. The comparison highlights the performance of traditional transform-based schemes, such as LWT-DCT and DWT-DCT, against the proposed method. As can be seen, the proposed approach achieves significantly lower embedding and extraction times, thanks to its optimized design and smaller watermark size, making it more suitable for real-time and hardware-focused implementations like FPGA and ASIC.

TABLE XIII. COMPARISON OF EMBEDDING AND EXTRACTION TIMES FOR EXISTING AND PROPOSED WATERMARKING METHODS

Reference Number	Host Image	Watermark Image	Embedding Time (s)	Extraction Time (s)
[6]	Lena (512×512)	CSIE (256×256)	LWT-DCT-0.4554 DWT-DCT-0.8776	LWT-DCT-0.5411 DWT-DCT-1.092
Proposed Method	Lena (512×512)	CSIE (128×128)	0.2321	0.0227

V. CONCLUSION

This work aimed to develop a watermarking technique that simultaneously achieves imperceptibility, robustness, capacity, and computational efficiency for real-time and hardware-oriented deployment. To address this, a hybrid DWT–DCT–SVD watermarking framework optimized using the Cheetah Optimization Algorithm was designed and evaluated. The method demonstrated significant advantages, achieving PSNR values above 55 dB, SSIM greater than 0.998, and near-perfect NCC under no-attack conditions indicating a clear improvement in imperceptibility as well as highly accurate watermark extraction when no distortions are applied. Robustness was validated under a wide range of image-processing and geometric distortions, with performance consistently superior or comparable to 4 existing watermarking schemes. The algorithm's structure consisting of fixed-size DWT, DCT, and SVD blocks, limited optimization iterations, and a moderate 128×128 watermark makes it well suited for FPGA and ASIC realization. The reduced embedding and extraction times further indicate its computational efficiency. Despite strong results, the approach exhibits reduced resistance under extreme noise conditions and carries increased computational load due to multiple transform stages, which may challenge very resource-limited hardware. Future research will focus on improving robustness against severe geometric and noise-based distortions, reducing hardware complexity, extending the method to color images and video watermarking, and validating power consumption and throughput through FPGA and ASIC prototyping.

CONFLICT OF INTEREST

The authors declare no conflict of interest.

AUTHOR CONTRIBUTIONS

SP conceptualized the study, developed the proposed DWT-DCT-SVD with Cheetah Optimization Algorithm (COA) watermarking method, and conducted the comparative analysis with existing techniques. VRK contributed to algorithm implementation, conducted robustness and imperceptibility evaluations, and assisted in the preparation and refinement of the manuscript. Both authors reviewed and approved the final version of the paper.

ACKNOWLEDGMENT

The authors gratefully acknowledge the Department of ECE, YSREC of Yogi Vemana University, Proddatur, for providing the necessary support, infrastructure, and resources throughout the course of this research work.

REFERENCES

[1] V. Varuikhin and A. Levina, "Continuous wavelet transform applications in steganography," *Procedia Computer Science*, vol. 186, pp. 580–587, 2021.

[2] V. Varuikhin and A. Levina, "Steganographic information hiding method based on continuous wavelet transform," in *Proc. 9th Mediterranean Conf. on Embedded Computing (MECO)*, 2020, pp. 1–4.

[3] V. Varuikhin and A. Levina, "Steganographic information hiding method based on double wavelet transform," in *Proc. 11th Mediterranean Conf. on Embedded Computing (MECO)*, 2022, pp. 1–5.

[4] D. Awasthi and V. K. Srivastava, "Robust, imperceptible and optimized watermarking of DICOM image using schur decomposition, LWT-DCT-SVD and its authentication using SURF," *Multimedia Tools and Applications*, vol. 82, pp. 16555–16589, 2023.

[5] D. Awasthi and V. K. Srivastava, "LWT-DCT-SVD and DWT-DCT-SVD based watermarking schemes with their performance enhancement using Jaya and particle swarm optimization and comparison of results under various attacks," *Multimedia Tools and Applications*, vol. 81, pp. 25075–25099, 2022.

[6] S. A. Barlaskar, A. M. Kirupakaran, R. H. Laskar *et al.*, "A robust digital image watermarking technique in LWT-DCT domain using particle swarm optimization and statistical distortion correction," *Multimedia Tools and Applications*, vol. 84, pp. 1429–1461, 2025.

[7] D. Rajani and P. R. Kumar, "An optimized hybrid algorithm for blind watermarking scheme using singular value decomposition in RDWT-DCT domain," *Journal of Applied Security Research*, vol. 17, no. 1, pp. 103–122, 2020.

[8] B. Mokashi, V. S. Bhat, J. D. Pujari *et al.*, "Efficient hybrid blind watermarking in DWT-DCT-SVD with dual biometric features for images," *Contrast Media & Molecular Imaging*, vol. 2022, no. 1, 2918126, 2022.

[9] K. Fares, A. Khaldi, K. Redouane *et al.*, "DCT & DWT based watermarking scheme for medical information security," *Biomedical Signal Processing and Control*, vol. 66, Art. no. 102403, 2021.

[10] V. Maheshkar, S. Kamble, S. Agarwal *et al.*, "Feature image generation using low, mid and high frequency regions for face recognition," *The International Journal of Multimedia & Its Applications (IJMA)*, vol. 4, no. 1, pp. 75–82, 2012.

[11] R. C. Gonzalez and R. E. Woods, *Digital Image Processing*, 4th ed. Delhi, India: Pearson India, 2019.

[12] I. A. Ansari, M. Pant, and C. W. Ahn, "ABC optimized secured image watermarking scheme to find out the rightful ownership," *Optik*, vol. 127, no. 14, pp. 5711–5721, 2016.

[13] T. T. Takore, P. R. Kumar, and G. L. Devi, "A modified blind image watermarking scheme based on DWT, DCT and SVD domain using

GA to optimize robustness," in *Proc. Int. Conf. Electrical, Electronics, and Optimization Techniques (ICEEOT)*, 2016, pp. 2725–2729.
[14] H. H. Tsai, Y. J. Jhuang, and Y. S. Lai, "An SVD-based image watermarking in wavelet domain using SVR and PSO," *Applied Soft Computing*, vol. 12, no. 8, pp. 2442–2453, 2012.
[15] P. P. Zheng, J. Feng, Z. Li *et al.*, "A novel SVD and LS-SVM combination algorithm for blind watermarking," *Neurocomputing*, vol. 142, pp. 520–528, 2014.
[16] N. Saxena, K. K. Mishra, and A. Tripathi, "DWT-SVD-based color image watermarking using dynamic-PSO," in *Proc. Advances in Computer and Computational Sciences*, 2018, pp. 343–351.
[17] S. J. O'Brien, W. E. Johnson, C. A. Driscoll *et al.*, "Conservation genetics of the cheetah: Lessons learned and new opportunities," *Journal of Heredity*, vol. 108, no. 6, pp. 671–677, 2017.
[18] L. Marker, L. K. Boast, A. Schmidt-Küntzel *et al.*, *Cheetahs: Biology and Conservation*, 1st ed., Amsterdam, Netherlands: Academic Press, 2017.
[19] P. R. Krausman and S. M. Morales, "Acinonyx jubatus," *Mammalian Species*, vol. 2005, no. 771, pp. 1–6, 2005.
[20] M. A. Akbari, M. Zare, R. Azizipanah-abarghooee *et al.*, "The cheetah optimizer: A nature-inspired metaheuristic algorithm for large-scale optimization problems," *Scientific Reports*, vol. 12, Art. no. 10953, 2022.
[21] P. Mohammadi, A. Ebrahimi-Moghadam, and S. Shirani, "Subjective and objective quality assessment of image: A survey," arXiv Preprint, arXiv:1406.7799, 2014.
[22] A. Kaur, J. S. Sidhu, and J. S. Bhullar, "Image quality assessment parameters: An overview," *Int. J. Res. Eng. Appl. Manag. (IJREAM)*, vol. 4, no. 4, pp. 125–127, 2018.
[23] C. S. Varnan, A. Jagan, J. Kaur *et al.*, "Image quality assessment techniques in spatial domain," *International Journal of Computer Science and Technology (IJCST)*, vol. 2, no. 3, pp. 177–184, 2011.
[24] Z. Wang and A. C. Bovik, "A universal image quality index," *IEEE Signal Process. Lett.*, vol. 9, no. 3, pp. 81–84, 2002.
[25] T. Samajdar and M. I. Quraishi, "Analysis and evaluation of image quality metrics," in *Proc. Information Systems Design and Intelligent Applications*, 2015, pp. 369–378.
[26] A. K. Boyat and B. K. Joshi, "A review paper: Noise models in digital image processing," arXiv Preprint, arXiv:1505.03489, 2015.
[27] C. Song, S. Sudirman, M. Merabti *et al.*, "Analysis of digital image watermark attacks," in *Proc. 7th IEEE Consumer Communications and Networking Conf.*, 2010, pp. 1–5.
[28] E. Hussein and M. A. Belal, "Digital watermarking techniques, applications and attacks applied to digital media: A survey," *International Journal of Engineering Research and Technology*, vol. 1, no. 7, pp. 1–8, 2012.
[29] P. Singh and R. S. Chadha, "A survey of digital watermarking techniques, applications and attacks," *International Journal of Engineering and Innovative Technology*, vol. 2, no. 9, pp. 165–175, 2013.
[30] S. Voloshynovskiy, S. Pereira, T. Pun *et al.*, "Attacks on digital watermarks: Classification, estimation based attacks, and benchmarks," *IEEE Communications Magazine*, vol. 39, no. 8, pp. 118–126, 2001.
[31] S. S. Al-amri, N. V. Kalyankar, and S. D. Khamitkar, "A comparative study of removal noise from remote sensing image," arXiv Preprint, arXiv: 1002.1148, 2010.
[32] N. S. Rekhi, J. S. Sidhu, and A. Arora, "Gamma correction for brightness preservation in natural images," *Computer Systems Science and Engineering*, vol. 44, no. 3, pp. 2791–2807, 2023.
[33] Z. Yu, Z. Ju, L. Teng *et al.*, "Large-capacity information hiding scheme based on minimum pixel modification," *Egyptian Informatics Journal*, vol. 23, no. 4, pp. 97–108, 2022.
[34] P. Puteaux, S. Y. Ong, K. S. Wong *et al.*, "A survey of reversible data hiding in encrypted images—The first 12 years," *Journal of Visual Communication and Image Representation*, vol. 77, 103085, 2021.
[35] I. Cox, M. Miller, J. Bloom *et al.*, *Digital Watermarking and Steganography*, 2nd ed. Burlington, USA: Morgan Kaufmann., 2007.
[36] D. Harris-Birtill and R. Harris-Birtill, "Understanding Computation Time: A Critical Discussion of Time as a Computational Performance Metric," in *Time in Variance*, 1st ed. vol. 17, A. Misztal, P. A. Harris, and J. A. Parker Eds. Leiden: Brill, 2022, pp. 220–248.
[37] Z. He, "Quality and computation time in optimization problems," arXiv Preprint, arXiv: 2111.10595, 2021.